

Effect of the Structure of Epoxy Monomers and Curing Agents: Toward Making Intrinsically Highly Thermally Conductive and Low-Dielectric Epoxy Resins

Junliang Zhang,[§] Lin Dang,[§] Fengyuan Zhang, Kuan Zhang, Qingqing Kong, and Junwei Gu*



Cite This: *JACS Au* 2023, 3, 3424–3435



Read Online

ACCESS |

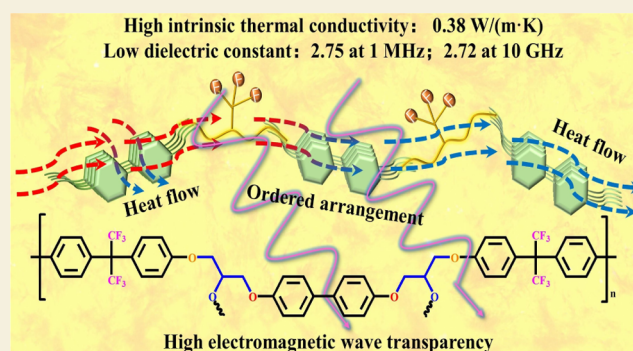
Metrics & More

Article Recommendations

Supporting Information

ABSTRACT: The low intrinsic thermal conduction and high dielectric properties of epoxy resins have significantly limited their applications in electrical and electronic devices with high integration, high frequency, high power, and miniaturization. Herein, a liquid crystalline epoxy (LCE) monomer with a biphenyl mesogenic unit was first synthesized through an efficient one-step reaction. Subsequently, bisphenol AF (BPAF) containing low-polarizable $-\text{CF}_3$ groups and 4,4'-diaminodiphenylmethane (DDM) were applied to cure the LCE and commercial diglycidyl ether of bisphenol A-type epoxy (E-51), respectively, to afford four kinds of epoxy resins with various intrinsic thermal conductivity and dielectricity values. Owing to the dual effect of microscopically stacking of mesogens and the contribution of fluorine to the formation of liquid crystallinity, ordered microstructures of the nematic liquid crystal phase were formed within the cross-linking network of LCE as confirmed by polarized optical microscopy and X-ray diffraction. Consequently, phonon scattering was suppressed, and the intrinsic thermal conductivity was improved considerably to $0.38 \text{ W}/(\text{m}\cdot\text{K})$, nearly twice as high as that of E-51 cured with DDM ($0.20 \text{ W}/(\text{m}\cdot\text{K})$). Additionally, the ordered microstructure and ultralow polar $-\text{CF}_3$ groups within LCE cured with BPAF enabled the epoxy resin to exhibit a remarkably lower and stable dielectric constant (ϵ) and dielectric loss tangent ($\tan \delta$) over both low and high frequencies compared to E-51 cured with DDM. The ϵ decreased from 3.40 to 2.72 while the $\tan \delta$ decreased from 0.044 to 0.038 at 10 GHz. This work presents a scalable and facile strategy for breaking the bottleneck of making epoxy resins simultaneously with high inherent thermal conduction and low dielectric performance.

KEYWORDS: epoxy resins, intrinsic thermal conductivity, liquid crystallinity, low polarity, fluorine, dielectric constant, dielectric loss, curing agent



1. INTRODUCTION

Nowadays, the rapid advancement of science and technology largely depends on the support of high-performance materials. Epoxy resins are widely utilized in electronic packaging, copper-clad plates, printed circuit boards, semiconductors, wireless base stations, and other electronic information, communication, and electrical fields ascribed to their high strength, superb electrical insulation, chemical corrosion resistance, low coefficient of linear expansion, low shrinkage, as well as easy processability and low cost.^{1,2} However, electronic and electrical devices are developing toward high density, high integration, high power, and miniaturization. Consequently, the packing density is also increasing exponentially.^{3–5} These inevitably cause the substantial increase of heat generation and accumulation,^{6,7} which would bring adverse effects to the stability, reliability, durability, and service life of components or even burnout or explosion in some extreme circumstances.^{8,9} Therefore, packaging materials and substrates with efficient heat dissipation are urgently required.^{10–12} In

addition, with the growth of high-speed and high-frequency communication technology, information processing and transmission should be very fast to ensure the stability and fidelity of electromagnetic signals and to avoid signal propagation delay, attenuation, and crosstalk. Therefore, the substrates and packaging materials should possess low dielectric constant (ϵ) and dielectric loss tangent ($\tan \delta$)^{13,14} values in addition to the efficient heat dissipation in order to address these pressing thermal management and electromagnetic wave transmission challenges.

Received: September 29, 2023

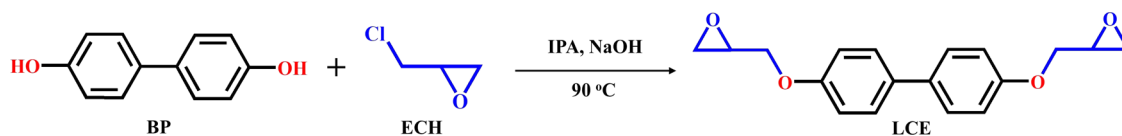
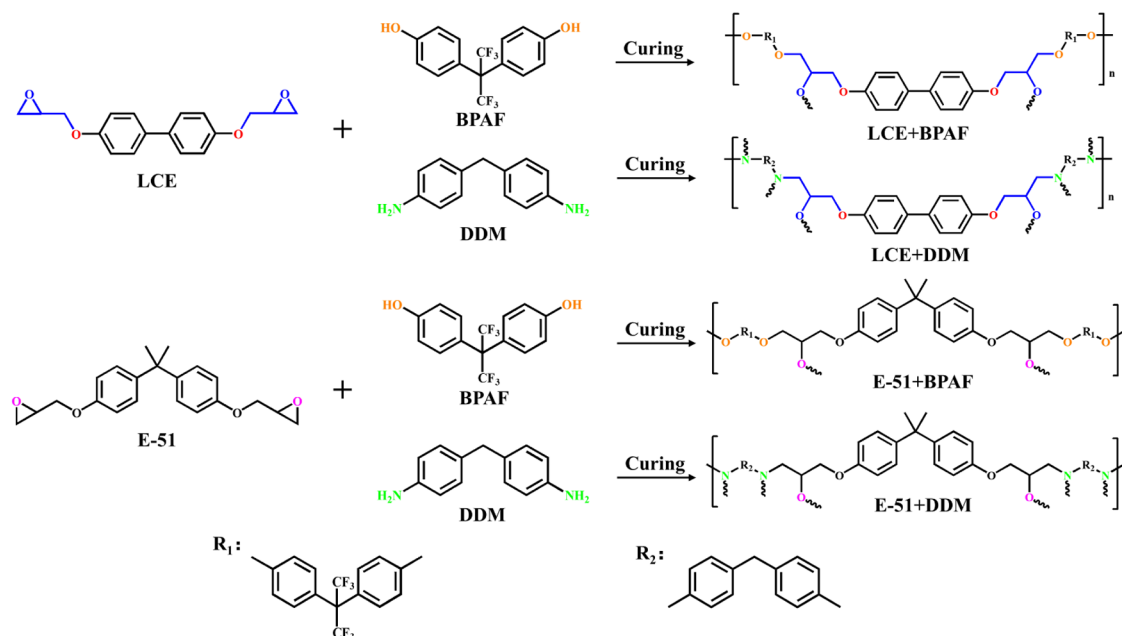
Revised: November 14, 2023

Accepted: November 16, 2023

Published: November 28, 2023



Scheme 1. Schematic Diagram of the Synthetic Route of LCE

Scheme 2. Schematic Diagram of the Synthetic Steps of Different Epoxy Resins (the Ether Group was Drawn for Simplicity because the Secondary Hydroxyl Group Generated by the Ring-Opening of the Epoxy Group Could Continue to React with Another Epoxy Group)¹⁵

However, conventional epoxy resins normally generate an unordered cross-linked network after curing, resulting in severe phonon scattering and thus a low inherent thermal conductivity of merely around 0.2 W/(m·K).^{16,17} Additionally, very polar groups including hydroxyl, imide, or ester will be generated alongside the ring-opening of the epoxy group during curing, hence forming dipole or interfacial polarization. Thereby, the ϵ and $\tan \delta$ will be increased, which in turn will cause the accumulation of heat to the substrate as $\tan \delta$ corresponds to the amount of electrical energy converted to heat under an external electric field.^{18,19} Meanwhile, it also leads to signal loss or distortion.²⁰ Therefore, developing epoxy resins with both high intrinsic thermal conductivity and low dielectricity will further broaden their applications and promote the development of high-tech electronic products. Nevertheless, most of the reported studies only focus singly on either the intrinsic thermal conductivity or the dielectric properties as it is still a tough challenge to balance high intrinsic thermal conductivity and low dielectric constant and dielectric loss.¹⁸

The thermal conductivities of polymers enhance with increasing the phonon mean free path, which is inversely correlated to the phonon scattering.^{21,22} Therefore, enhancing the degree of crystallinity or the molecular chain orientation of polymers is considered an effective means of increasing the phonon mean free path.²³ Previous researchers mainly introduced liquid crystal units¹⁷ such as biphenyl,²⁴ fused benzene rings,²⁵ or aryl esters^{26,27} into epoxy monomers or curing agents²⁸ to improve the regularity of the microstructure

within the cross-linking network of epoxy resins. The phonon scattering is then suppressed through the formation of π - π stacking, thus enhancing the intrinsic thermal conductivity.²⁹ In addition, the ordered arrangement will inhibit the occurrence of dipole polarization, thereby decreasing the dielectric permittivity and dielectric loss. However, introducing a liquid crystal group into the epoxy molecule usually requires multistep reactions and tedious purification processes,²⁵ which prolongs the duration of synthesis and increases the cost of use, not to mention the difficulty of scaling up. The enhancement of the intrinsic thermal conduction of epoxy resins can also be realized by adjusting the way of curing or the topology of the polymer network. Jang et al.³⁰ used a cationic initiator instead of a traditional amine cross-linker to linearly weave epoxy groups, which were tethered to the aligned liquid crystalline units. The intrinsic thermal conduction of the obtained epoxy resins was enhanced by 141%. Zhang et al.³¹ fabricated an interlocked liquid crystalline epoxy (LCE) copolymer network through topological reorganization enabled by the dynamic Schiff base bond and the Diels–Alder bond. The thermal conduction of the interlocked polymer network was improved to 0.329 W/(m·K) from 0.218 and 0.255 W/(m·K) of the parent single polymer networks.

According to the Debye equation,³² the dielectric constant and dielectric loss of polymers can be reduced by introducing chemical bonds or functional groups with low molecular polarizability, increasing the proportion of free volume, or by introducing porous structures to decrease the polar molecule number per unit volume.^{13,33–35} For instance, by introducing

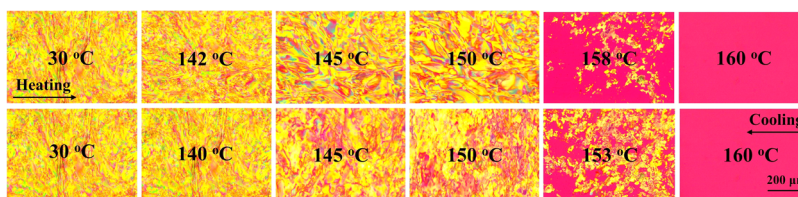


Figure 1. POM images of LCE taken at different temperatures of the heating and cooling steps.

polyhedral oligomeric silsesquioxanes (POSS),³⁶ a kind of organic–inorganic hybrid material containing a nanoporous structure, researchers have prepared epoxy resins with a low dielectric constant and dielectric loss.¹⁴ However, POSS are usually very expensive. Besides, there is always an interface generated between the inorganic phase and the organic phase, resulting in severe interfacial polarization, which is unfavorable to the reduction of dielectric permittivity. Furthermore, the introduction of porous structures will hinder the close-packing interactions of molecular chains within the cross-linking network. This will cause an aggravation of phonon scattering and decrease the thermal conductivity. As is known, the ring-opening reaction between an amine and an epoxy group will generate highly polar hydroxyl groups. In order to avoid this reaction, Zhang et al.² synthesized a series of bifunctional silylamines to copolymerize with E-51. Due to the silylotropic N-to-O migration, which forms low-polar silyloxy rather than the hydroxyl group, the epoxy copolymers exhibited remarkably low ϵ and $\tan \delta$. Furthermore, researchers also prepared epoxy resins with low dielectric properties by applying an anhydride curing agent³⁷ or introducing imide moieties³⁸ and low-polarizable C–Si^{39,40} or C–F^{41–43} bonds. Meanwhile, introducing fluorine has been shown to greatly increase the formation of liquid crystallinity,¹⁹ thereby enhancing the heat conduction efficiency. However, making epoxy resins simultaneously with increased intrinsic thermal conduction and very low dielectric properties is still challenging and has rarely been reported so far.

In this work, an LCE monomer containing a biphenyl mesogenic unit was first synthesized through a facile and efficient one-step reaction (Scheme 1). Subsequently, commercially available low-polarizable $-\text{CF}_3$ groups containing bisphenol AF (BPAF) and 4,4'-diaminodiphenylmethane (DDM) were applied as cross-linkers to cure LCE and commercial E-51, respectively, to prepare four kinds of epoxy resins with various intrinsic thermal conductivity and dielectricity values (samples denoted as LCE + BPAF, LCE + DDM, E-51 + BPAF, and E-51 + DDM, Scheme 2). The effect of the structures of epoxy monomers and curing agents regarding the intrinsic thermal conductivity, dielectric properties, insulation performance, thermomechanical properties, thermal stability, and hydrophobicity of the prepared epoxy resins was systematically explored. This study presents a convenient and scalable method for preparing epoxy resins that simultaneously exhibit a high intrinsic thermal conductivity and low dielectric performance. The developed materials are expected to find prosperous applications in the fields of electronic packaging, copper-clad plates, and printed circuit boards, which require both very low permittivity and high intrinsic thermal conductivity for a high quality of electromagnetic signal transmission and effective heat dissipation.

2. EXPERIMENTAL SECTION

2.1. Materials

4,4'-Dihydroxybiphenyl (BP, 97%), epichlorohydrin (ECH, 98%), and bisphenol AF (BPAF, 98%) were purchased from Shanghai Aladdin Biochemical Technology Co., Ltd. (Shanghai, China). Isopropyl alcohol (IPA, 99.5%) and 4,4'-diaminodiphenylmethane (DDM, 97%) were obtained from Shanghai Macklin Biochemical Co., Ltd. (Shanghai, China). Sodium hydroxide (NaOH, analytical grade) and absolute ethanol (EtOH, analytical grade) were supplied by Guangdong Guanghua Technology Co., Ltd. (Guangdong, China). Bisphenol A epoxy resin (E-51, chemically pure) was purchased from Laizhou Baichen Insulation Materials Co., Ltd. (Shandong, China). All of the materials were used as received without further treatment.

2.2. Synthesis of the Liquid Crystalline Epoxy (LCE) Monomer

The synthetic step of LCE is shown in Scheme 1. Specifically, BP (10 g, 54 mmol), deionized water (9.5 mL), IPA (33 mL), and ECH (42.5 mL, 64.2 mmol) were added to a three-necked flask equipped with a stirring bar and then put into an oil bath at 90 °C. After the mixture became transparent, 9.5 mL of NaOH solution (4.65 g of NaOH dissolved in 19 mL of water) was added dropwise within 1 h. The reaction was then proceeded for 1 h, and the remaining NaOH solution was added dropwise within 1 h. Then, the reaction was continued for one more hour. After the reaction, the mixture was cooled to room temperature and a large amount of solid was precipitated. The solid was filtered and washed sequentially with water, ethanol–water mixture (1:1 by volume), and ethanol. The product of LCE was obtained after drying in an oven at 60 °C as a white solid with a yield of 89.7%.

2.3. Preparation of Different Epoxy Resins

A certain amount of LCE and BPAF (the molar ratio of hydroxyl group to epoxy group was 1:1) was mixed and heated to 120 °C to melt and then stirred evenly; then, it was poured into a preheated mold of 120 °C. The mixture was degassed under a vacuum and cured at 150 °C for 4 h without applying pressure to obtain the cured epoxy resin (denoted as LCE + BPAF). The other epoxy resins of LCE cured with DDM (denoted as LCE + DDM), E-51 cured with BPAF (denoted as E-51 + BPAF), and E-51 cured with DDM (denoted as E-51 + DDM) were prepared with a stoichiometric amount according to the same procedures with LCE + BPAF. In order to compare the effect of the curing temperature to the thermal conductivity and dielectricity of the epoxy resins, control samples cured at 180 °C were also prepared following the same procedure described above.

3. RESULTS AND DISCUSSION

3.1. Characterization and Liquid Crystalline Behavior of LCE

LCE possessed the simplest mesogen unit, and its structure was confirmed by ¹H and ¹³C nuclear magnetic resonance (NMR, Figure S1) as well as Fourier transform infrared (FT-IR, Figure S2) spectroscopy. The liquid crystalline behavior of LCE was first investigated using differential scanning calorimetry (DSC) analysis and polarized optical microscopy (POM). The DSC curves of the LCE (Figure S3) showed two peaks during both the heating and cooling stages. The

Table 1. DMA and TGA Data of LCE + DDM, E-51 + DDM, LCE + BPAF, and E-51 + BPAF Resins Cured at 150 °C

samples	weight loss temperature (°C)		<i>a</i>		<i>b</i>			final carbon residue (wt %)
	5 wt %	30 wt %	$T_{\text{Heat-resistance index}}^a$ (°C)	T_g (°C)	E^{*b} (MPa)	ν_e (mol m ⁻³)		
LCE + DDM	340.0	366.0	174.2	199.0	1977.1	3758.2	22.5	
E-51 + DDM	348.0	373.4	178.0	182.0	1423.7	1948.2	13.1	
LCE + BPAF	288.4	409.4	176.9	137.4	1712.9	32.7	12.4	
E-51 + BPAF	249.8	408.7	169.1	124.0	1832.2	26.8	7.1	

^a $T_{\text{Heat-resistance index}} = 0.49 \times [T_5 + 0.6 \times (T_{30} - T_5)]$, where T_5 and T_{30} correspond to temperatures of 5 and 30 wt % weight loss, respectively. ^bData at 30 °C.

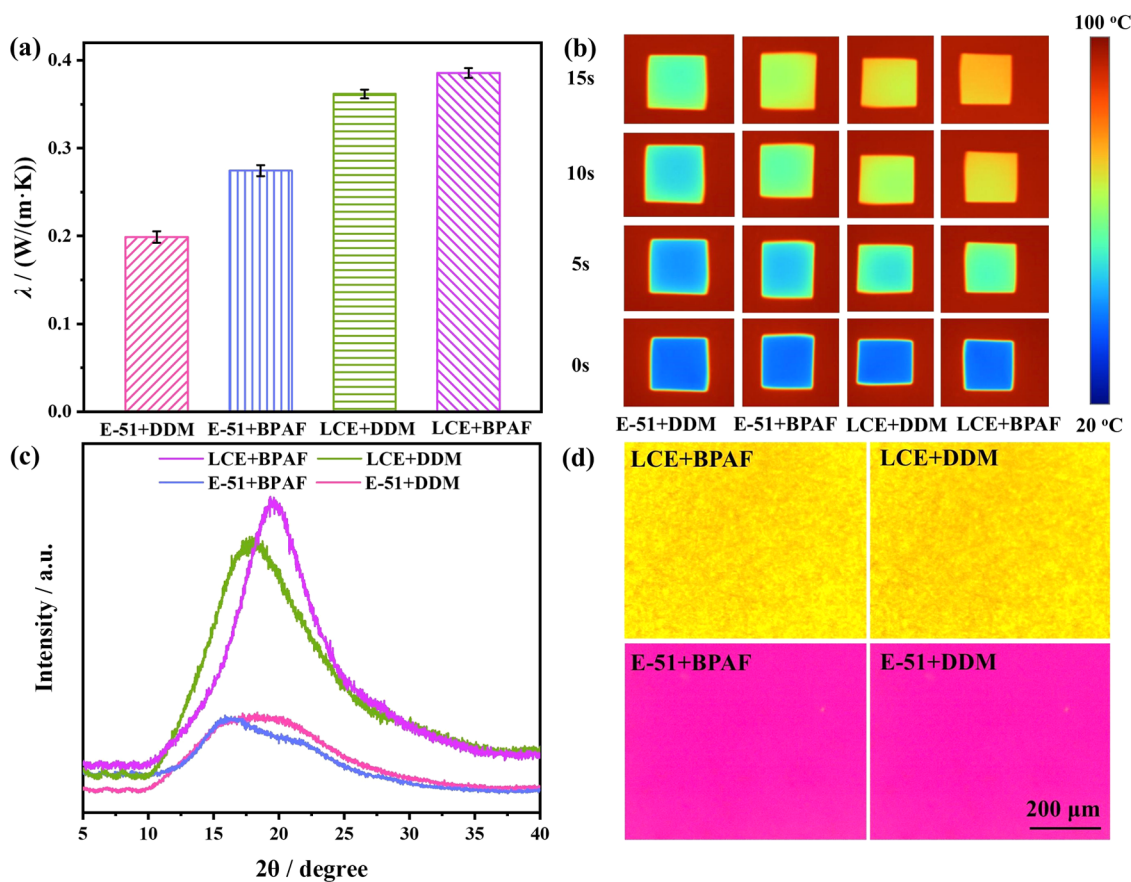


Figure 2. Thermal conductivities (a), infrared thermal imaging photos (b), XRD curves (c), and POM images at 25 °C (d) of E-51 + DDM, E-51 + BPAF, LCE + DDM, and LCE + BPAF resins cured at 150 °C.

endothermic peak at 149 °C during heating corresponded to the transformation of LCE from the crystal state to the liquid crystal phase, while the peak at 154 °C indicated the transformation from the liquid crystal phase to the isotropic liquid state. The two endothermic peaks of 145 and 137 °C during the cooling process corresponded to the conversion from the isotropic liquid state to the liquid crystal stage and then to the crystal stage, respectively. Meanwhile, as shown in the POM images (Figure 1) taken at different temperatures during the heating process, the crystalline phase was observed at 30 °C as LCE exhibited a clear birefringence as observed in the visual area. As the temperature was raised to 142 °C, LCE showed a fluidic feature, implying the emergence of the liquid crystal phase. As the temperature increased higher, the birefringence decreased gradually and completely disappeared until the isotropic liquid state at 160 °C. Notably, this phenomenon was reversible as a similar but reverse trend was observed upon cooling. The DSC and POM analyses were

consistent, both indicating that LCE was bidirectional thermotropic liquid crystalline, and the liquid crystal forming temperature window was 142–158 °C.

3.2. Curing Behaviors of Different Epoxy Resins

The curing behaviors of LCE and E-51 cured with BPAF and DDM were first investigated by dynamic DSC (Figure S4). In contrast to the DDM-cured epoxy resins, which showed exothermic reactions starting from ~ 100 °C, the BPAF-cured epoxy resins exhibited curing reactions beginning at ~ 165 °C at the heating rate of 10 °C/min. Besides, the LCE + BPAF resin showed the highest exothermic peak temperature of 263 °C, followed by 238, 157, and 136 °C of E-51 + BPAF, LCE + DDM, and E-51 + DDM resins, respectively.

This is because, on the one hand, the nitrogen atom on the amine group in DDM contains lone-pair electrons, where the electron cloud density is high. Thus, nitrogen is more likely to attacking the electron-deficient carbon atom in the epoxy

group, resulting in the nucleophilic ring-opening reaction. On the other hand, there is a conjugation effect between the phenolic hydroxyl group and the benzene ring in BPAF, and the electron cloud density around the hydroxyl group is relatively low, which is not conducive to attack the electron-deficient carbon atom in the epoxy group. However, the phenolic hydroxyl group is acidic and can provide protons; therefore, the hydrogen atom in the phenolic hydroxyl group can combine with the oxygen atom in the epoxy group, leading to an electrophilic ring-opening reaction. Due to the higher electron cloud density around the nitrogen atom, DDM has a higher reactivity with the epoxy group than BPAF, resulting in the higher exothermic curing reaction peak temperatures of LCE and E-51 when cured with BPAF. Furthermore, since LCE contains a biphenyl group, it causes a stronger conjugation effect with the epoxy group than E-51. Consequently, the electron cloud density in the oxygen atom of the epoxy group in LCE is relatively lower; thus, the electrophilic ring-opening reaction is more difficult to occur. Therefore, the exothermic peak temperature of LCE + BPAF was the highest, while that of E-51 + DDM was the lowest. In addition, the exothermic peaks of LCE and E-51 cured with DDM were much stronger, indicating a more intense curing reaction and higher cross-linking density (confirmed by dynamic mechanical analysis (DMA), Table 1).

3.3. Thermal Conductivities of Different Epoxy Resins

In order to obtain high thermal conduction, LCE should be cured within the liquid crystalline formation temperature window so as to maintain the ordered liquid crystalline structure.²² Therefore, 150 °C was selected to be the curing temperature for LCE as it exhibited the most liquid crystalline state as confirmed by POM. In order to keep the curing conditions consistent and the results comparable, E-51 was also cured at 150 °C. It is worth mentioning that the optimal temperatures for the curing reactions of LCE and E-51 with BPAF were higher than 150 °C. Therefore, the curing duration was extended to ensure complete curing for all of the resins. According to Fourier transform infrared (FT-IR) spectroscopy (Figure S5), the curing of all of the epoxies could be fully completed after 4 h because the characteristic peaks of epoxy groups at 913 cm⁻¹ disappeared completely. Besides, the signal at around 3400 cm⁻¹ associated with the hydroxyl groups in BPAF and E-51 weakened gradually as the curing reaction proceeded. It needs to be noted that secondary hydroxyl groups would be generated after the epoxy ring-opening.³⁹ The absence of the signal after curing might be ascribed to the very small amount of hydroxyl groups, which cannot be detected. The epoxy resins after curing were then analyzed by DSC, and no remaining curing exothermic peak was evident from the thermograms of the heating process (Figure S6), confirming all of the epoxies were fully cured.^{22,44,45} Besides, no increase of the storage modulus (*E'*) was observed when heated during the DMA test (see below), which further confirmed the complete curing of all of the epoxy resins (cured samples shown in Figure S7).

As shown in Figure 2a, the cured epoxy resin of LCE + BPAF exhibited the highest thermal conductivity (λ) of 0.38 W/(m·K), which was approximately two times higher compared to the 0.20 W/(m·K) of the conventional E-51 + DDM resin. Meanwhile, the LCE + DDM and E-51 + BPAF resin systems showed λ values of 0.36 and 0.28 W/(m·K), respectively. The infrared thermal imaging in Figure 2b

exhibited a consistent result. The LCE + BPAF resin showed the highest surface temperature when heated for the same time and demonstrated the fastest heating rate by reaching 80 °C after 15 s (Figure S8), confirming it had the highest thermal conduction capacity.

The lower thermal conductivities of cured E-51-based epoxy resins were due to the absence of liquid crystallinity, where no ordered regions were formed to reduce phonon scattering. The enhancement of thermal conductivity for LCE + BPAF originated from the highly oriented biphenyl mesogen packing structures with π - π interactions within the cured network. Consequently, random orientation of the molecular chains was reduced, and thereby, the phonon scattering was suppressed and minimized because of the harmonic molecular lattice vibrations through the ordered liquid crystalline structure. Consequently, the heat conduction efficiency will be greatly improved, making the λ value higher than that of the cured resin without LCE. In contrast, the ordered mesogenic structure was distorted to some extent when LCE was cross-linked with DDM as the amine and epoxy groups formed a restricted bond angle;³⁰ thus, stronger phonon scattering will be caused, leading to a slightly lower thermal conductivity. On the other hand, fluorine is conducive to the formation of liquid crystallinity within the network of LCE cured with BPAF, providing more pathways for thermal conduction and resulting in a higher thermal conductivity. It should be noted that due to the amorphous regions presented in the network of cured LCE resins, the domains of microscopic anisotropic structures formed by ordered mesogens would be disordered. Therefore, the thermal conductivities were macroscopically isotropic for LCE-based epoxy resins.

In order to further investigate the connection between the microstructure and thermal conduction of the cured epoxy resins, an X-ray diffraction (XRD) analysis was conducted (Figure 2c). In contrast to the E-51 + BPAF and E-51 + DDM resins, which showed a broad diffuse peak, implying the formation of an amorphous microstructure within the copolymer matrix, a strong diffraction peak at $2\theta = 19.4$ and 17.6° corresponding to peaks of uncured LCE (Figure S9) was observed for LCE + BPAF and LCE + DDM resins, respectively. This revealed the presence of a regular crystal-like structure within the cured networks, suggesting that the liquid crystalline structure was successfully frozen. Besides, no signals were present in the small angles of $2\theta = 5$ – 10° in the XRD curves, which proved the formation of a nematic liquid crystalline phase.⁴⁶ It is noteworthy that the diffraction peaks of cured LCE-based samples were weaker compared with that of the LCE monomer. This is ascribed to the fact that the curing agents that lack the mesogenic units will make the mesogenic groups hard to aggregate on a large scale and the cross-linked network will also generate hindrance for the formation of ordered regions.³¹ However, a smaller scale of regular regions was still formed due to the irresistible tendency of mesogen aggregating. Furthermore, the interplanar spacings between the mesogenic units of LCE + BPAF and LCE + DDM resins calculated by the Bragg formula⁴⁷ ($2d \sin \theta = n\lambda$, where λ is the wavelength) were 0.457 and 0.498 nm, respectively, which demonstrated a higher density of crystallinity in the cured network of LCE + BPAF than LCE + DDM. POM was further employed to characterize the microstructure of the cured epoxy resins (Figure 2d). LCE + BPAF and LCE + DDM exhibited a birefringence pattern at room temperature (25 °C), suggesting a crystal-like phase

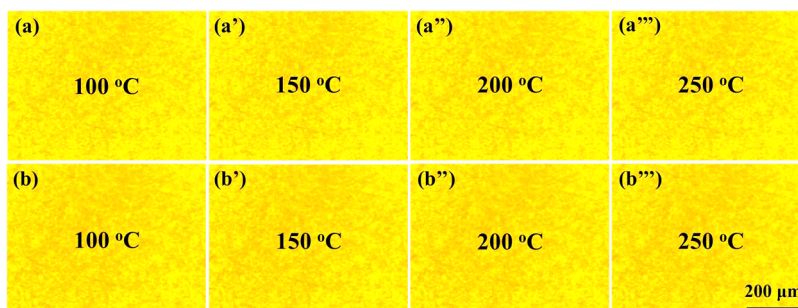


Figure 3. Dynamic POM images taken at different temperatures between 100 and 250 °C during heating (heating rate was 10 °C/min) of LCE + BPAF (a–a''') and LCE + DDM (b–b''') resins cured at 150 °C.

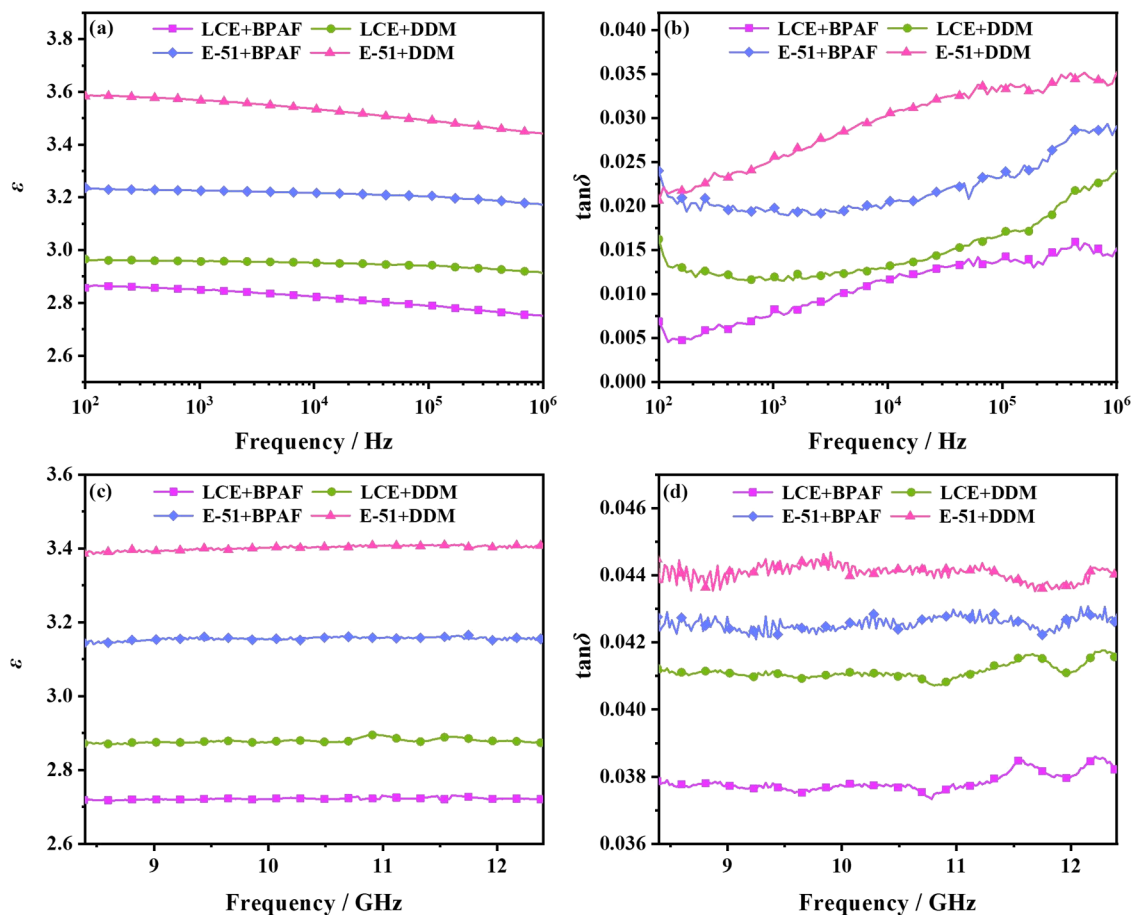


Figure 4. The ϵ (a, c) and $\tan \delta$ (b, d) values of LCE + BPAF, LCE + DDM, E-51 + BPAF, and E-51 + DDM resins cured at 150 °C at 10^2 – 10^6 Hz and 8.4–12.4 GHz, respectively.

structure, whereas no birefringence was observed for E-51 + BPAF and E-51 + DDM resins at both 25 °C and higher temperatures (Figure S10). Notably, the birefringence characteristic remained unchanged when LCE + BPAF and LCE + DDM were heated to 250 °C (Figure 3), indicating that the ordered liquid crystalline microstructure was successfully fixed and thus the efficiency of phonon transport was enhanced.

In order to address the importance of temperature on the formation of the liquid crystalline phase, the epoxy resins cured at 180 °C, which were out of the liquid crystalline formation temperature window of LCE, were also analyzed by XRD. As revealed in Figure S11, broad diffuse peaks were present for LCE + BPAF and LCE + DDM resins, indicating that the

epoxy resins were amorphous, which would enhance the phonon scattering and cause a decrease of the heat transfer efficiency. This can be confirmed by the lower thermal conductivities of 0.31 and 0.29 W/(m·K) for LCE + BPAF and LCE + DDM resins cured at 180 °C, respectively (Figure S12). It is worth mentioning that nearly identical peaks and thermal conductivities were displayed for E-51 + BPAF and E-51 + DDM resins cured at 180 °C (Figures S11 and S12) to those cured at 150 °C, demonstrating the amorphous microstructure was not affected by temperature. These results highlighted that temperature was a critical factor for the formation of a well-ordered liquid crystalline structure.

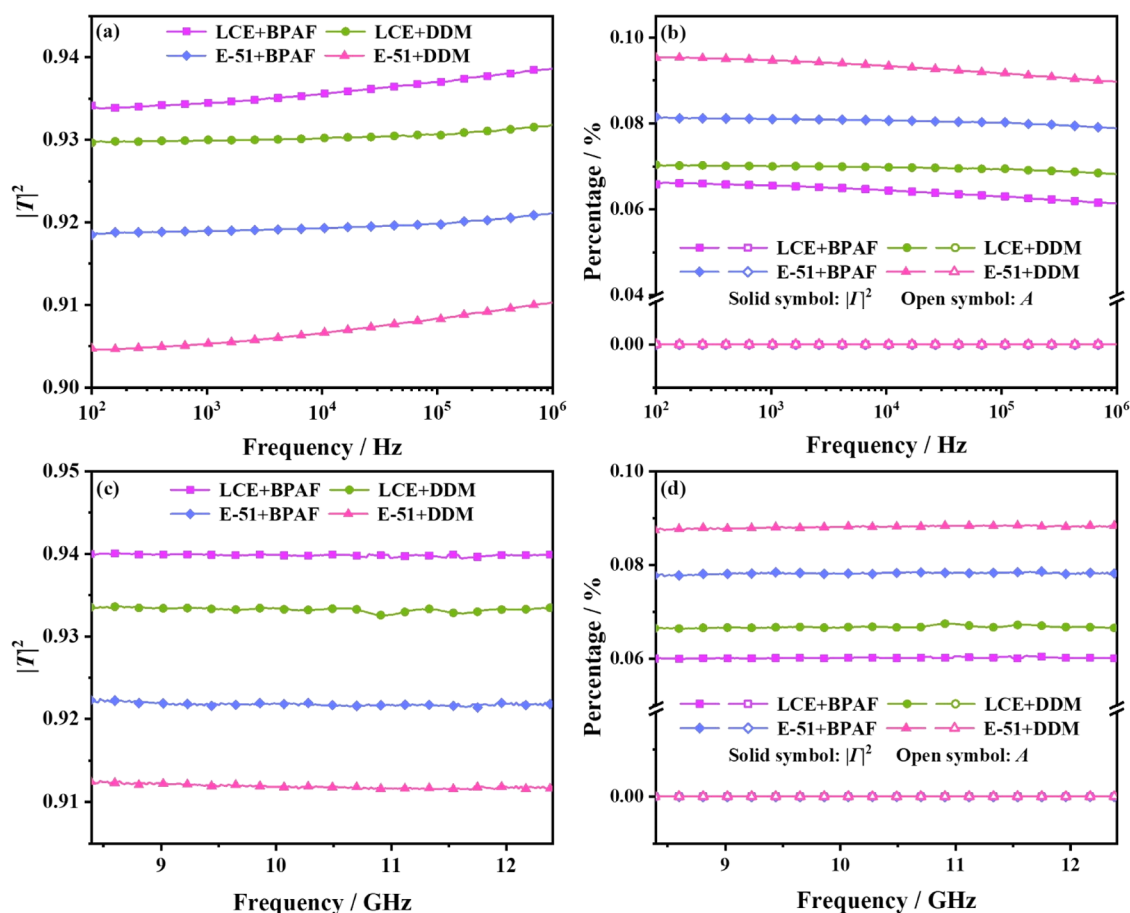


Figure 5. Theoretical $|T|^2$, $|\Gamma|^2$, and A values of LCE + BPAF, LCE + DDM, E-51 + BPAF, and E-51 + DDM resins cured at 150 °C at 10^2 – 10^6 Hz (a, b) and 8.4–12.4 GHz (c, d).

3.4. Dielectric Performance of Different Epoxy Resins

The dielectric performance (ϵ and $\tan \delta$) of the four epoxy resins at the low frequency of 10^2 – 10^6 Hz and high frequency of 8.4–12.4 GHz are displayed in Figure 4. As expected, the LCE + BPAF resin showed the lowest ϵ and $\tan \delta$ values at both low and high frequencies, remarkably lower than those of commercial E-51 cured with the DDM resin. Specifically, the LCE + BPAF resin exhibited a ϵ value of 2.75 and a $\tan \delta$ value of 0.015 at 10^6 Hz, while LCE + DDM, E-51 + BPAF, and E-51 + DDM resins demonstrated ϵ values of 2.91, 3.17, and 3.44, and $\tan \delta$ values of 0.024, 0.029, and 0.035, respectively (Figure 4a,b). For the high frequency of 10 GHz, the ϵ and $\tan \delta$ values of LCE + BPAF were 2.72 and 0.038, while the ϵ and $\tan \delta$ values of LCE + DDM, E-51 + BPAF, and E-51 + DDM resins were 2.87, 3.15, and 3.40, and 0.041, 0.042, and 0.044, respectively (Figure 4c,d).

It is worth mentioning that at the low frequency of 10^2 – 10^6 Hz, the ϵ values of the four epoxy resins decreased slightly with the increase of frequency. This is ascribed to the fact that the electron, atomic, and dipole polarization can catch up with the change of the electric field at lower frequencies, whereas only the electron polarization and atomic polarization can catch up with the change of the electric field at higher frequencies, resulting in decreased ϵ .⁴⁸ In addition, all four epoxy resins exhibited fluctuating $\tan \delta$ values, which might be caused by the dipolar relaxation.⁴⁹ Notably, the LCE + BPAF resin exhibited not only ultralow but also very stable ϵ and $\tan \delta$ values at high frequencies of 8.4–12.4 GHz, which is quite

essential for both high-speed and high-frequency circuit applications to ensure reliability during operation. Excitedly, the LCE + BPAF resin showed an even lower ϵ value than some common commercial low-dielectric polymeric materials, for instance, cyanate ester resin ($\epsilon \sim 3.0$),³⁴ polyimide ($\epsilon \sim 3.1$), and benzocyclobutene resin ($\epsilon \sim 2.8$).⁵⁰

The decreased ϵ and $\tan \delta$ of LCE + BPAF was mainly caused by the reduction of the dipole polarity ascribed to the low polarizable $-\text{CF}_3$ groups, which weakened the polarization of electrons resulting from the external electric field.⁵¹ Besides, the regular biphenyl liquid crystal mesogens improved the ordering of the cured network, which reduced the dipole polarization in the cured resin. This effect can be verified by the higher ϵ of 2.84 and $\tan \delta$ of 0.018 at 10^6 Hz when LCE was cured with BPAF at 180 °C (Figure S13), where an amorphous microstructure was demonstrated. However, the ϵ and $\tan \delta$ of E-51 cured at 180 °C with either BPAF or DDM remained unchanged. Additionally, the fluorine atom in BPAF had a large molecular free volume,⁵² resulting in the decreased density of dipoles. Furthermore, the rigid biphenyl structure restricted the mobility of the chain segment, which caused the reduction of distortion polarization. The above factors jointly endowed the LCE + BPAF resin with the lowest ϵ and $\tan \delta$ values. Besides, the effect of temperature on ϵ and $\tan \delta$ of all epoxy resins was further explored between 20 and 240 °C under the frequency of 1 MHz (Figure S14). Excitingly, both the ϵ and $\tan \delta$ of LCE-based epoxy resins remained constant during the whole temperature range. These results

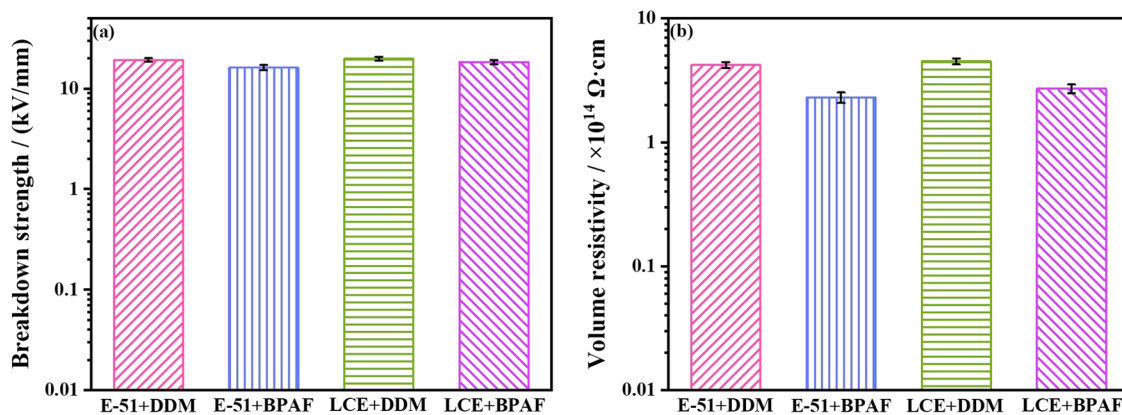


Figure 6. Electrical breakdown strength (a) and volume resistivity (b) of E-51 + DDM, E-51 + BPAF, LCE + DDM, and LCE + BPAF resins cured at 150 °C.

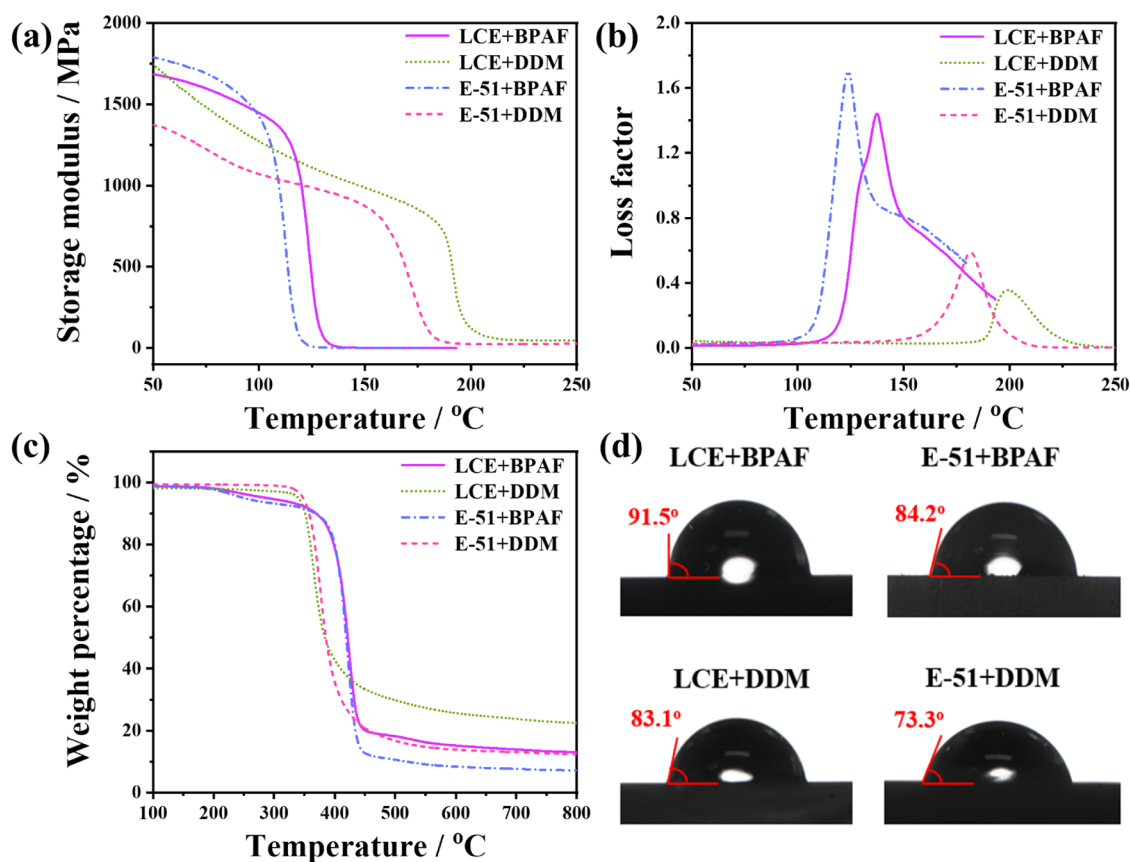


Figure 7. Storage modulus (a), loss factor (b), TGA curves (c), and water contact angle values (d) of LCE + BPAF, LCE + DDM, E-51 + BPAF, and E-51 + DDM resins cured at 150 °C.

suggest that the dielectric properties of LCE-based epoxy resins possessed good temperature stability at 1 MHz. This can be ascribed to the rigid biphenyl mesogens and the ordered microstructure that restrict the thermal motions of molecular chains and dipolar polarization. It is worth mentioning that E-51-based epoxy resins also held the ϵ and $\tan \delta$ values during the whole temperature range. This might be caused by the complete curing and the high cross-linking density (Table 1), which reduce the dipolar polarization.

When transmitting through the dielectrics, electromagnetic wave reflection on the surface and energy loss inside the material would occur, resulting in electromagnetic wave loss. The theoretical electromagnetic wave transmittance ($|T|^2$),

reflection coefficient ($|\Gamma|^2$), and energy loss (A) can be calculated by eqs 1–3⁵³ in accordance with the law of conservation of energy.

$$A = \frac{2\pi d \epsilon \tan \delta}{\lambda(\delta - \sin^2 \theta)^{1/2}} \quad (1)$$

$$|\Gamma|^2 = \left[\frac{(\epsilon - \sin^2 \theta)^{1/2} - \epsilon \cos \theta}{(\epsilon - \sin^2 \theta)^{1/2} + \epsilon \cos \theta} \right]^2 \quad (2)$$

$$A + |T|^2 + |\Gamma|^2 = 1 \quad (3)$$

where θ represents the electromagnetic wave incident angle, d corresponds to the dielectric material thickness, λ is the electromagnetic wavelength, and ε and $\tan \delta$ are the dielectric constant and dielectric loss tangent values of the dielectric material, respectively. According to these equations, $|T|^2$ is inversely correlated with the values of ε and $\tan \delta$. Therefore, decreasing ε and $\tan \delta$ will improve the wave transmittance. As displayed in Figure 5, the LCE + BPAF resin had the lowest $|T|^2$ and the highest $|T|^2$ of 93.9% at 10^6 Hz, higher than those of LCE + DDM, E-51 + BPAF, and E-51 + DDM resins, which were 93.2, 92.1, and 91.0%, respectively. Besides, the $|T|^2$ of the LCE + BPAF resin was 94.0% at the high frequency of 8.4–12.4 GHz, which was also higher than 93.3, 92.2, and 91.2% of LCE + DDM, E-51 + BPAF, and E-51 + DDM resins, respectively. This can be explained by the impedance matching theory.⁵⁴ The smaller the impedance difference between the load phase and the transmission phase (air), the lesser the reflection that occurs. Besides, the lower the $\tan \delta$, the lesser the energy that would be dissipated. Therefore, the lowest ε of the LCE + BPAF resin represented the smallest impedance difference between the transmission phase and the epoxy resin, thereby illustrating the lowest $|T|^2$ and the highest $|T|^2$. In addition, the A values of all of the epoxy resins were way lower compared with $|T|^2$ (Figure 5b,d), implying reflection loss was the main way that caused the electromagnetic wave energy reduction.

3.5. Electrical Performance of Different Epoxy Resins

The electrical breakdown strength and volume electrical resistivity of different epoxy resins were also explored. As shown in Figure 6a, there was a marginal difference among the breakdown strength values of 18.36, 19.83, 16.17, and 19.25 kV/mm for LCE + BPAF, LCE + DDM, E-51 + BPAF, and E-51 + DDM resins, respectively. Besides, the volume electrical resistivity of all four epoxy resins exceeded 10^{13} Ω -cm. The volume resistivity (Figure 6b) of the LCE + BPAF resin was 2.7×10^{14} Ω -cm, which was slightly lower than 4.5×10^{14} and 4.2×10^{14} Ω -cm for the LCE + DDM resin and the E-51 + DDM resin, respectively, but slightly higher than 2.3×10^{14} Ω -cm of the E-51 + BPAF resin. The biphenyl mesogen containing LCE formed an ordered and low polarizable network, which increased the electrical insulation. Besides, the cross-linking density of the epoxy resin cured with DDM was higher than that cured with BPAF (see below in Table 1), which reduced the defects of the curing network and thus increased the volume resistivity. However, the conjugated effect between the regular biphenyl units of LCE would facilitate electron transfer, which would decrease the volume electrical resistivity. Therefore, the LCE + DDM resin had the highest electrical breakdown strength and volume resistivity. Nevertheless, the LCE + BPAF resin exhibited comparable and desirable electrical insulation performance with respect to the commercial E-51 resin, as materials are generally considered to be insulating if the volume resistivity is higher than 10^{12} Ω -cm.⁵⁵

3.6. Thermomechanical and Thermal Property and Hydrophobicity of Different Epoxy Resins

The thermomechanical and thermal behaviors were examined with DMA and thermal gravimetric analysis (TGA), and the characteristic data are presented in Table 1. In comparison with the commercial E-51 cured with DDM, other three epoxy resins showed a much improved storage modulus (E') in the glassy region (Figure 7a). The E' values of LCE + DDM, E-51

+ BPAF, LCE + BPAF, and E-51 + DDM resins were 1977.1, 1832.2, 1712.9, and 1423.7 MPa at 30 °C, respectively. The highest E' value of LCE + DDM could be ascribed to the rigid biphenyl liquid crystal unit of LCE, the enlarged molecular free volume by C–F bonds, and the highest cross-linking density (ν_e ,⁵⁶ Table 1), which facilitated the load transfer. Additionally, the LCE + DDM resin showed the highest glass-transition temperature (T_g , determined from the peak temperature of the loss factor in Figure 7b) of 199.0 °C, while E-51 + DDM, LCE + BPAF, and E-51 + BPAF resins exhibited gradually decreased T_g values of 182.0, 137.4, and 124.0 °C, respectively. This can be partly ascribed to the regular arrangement of the rigid biphenyl unit in LCE. Besides, the epoxy resins cross-linked with DDM had a higher cross-linking density than BPAF. These two factors would restrict the chain movement to increase the T_g . However, the large free volume of the $-\text{CF}_3$ group was beneficial for the chain end movement, which caused a decrease of T_g . Consequently, LCE + DDM exhibited the highest T_g . It is noteworthy that, due to the strong electronegativity of fluorine and the high energy of C–F bonds, the intermolecular interactions increase, thus restricting the movement of molecular chains. It will cause phase lag between stress and strain, significantly increase the loss factor and loss modulus, and extend the damping temperature range. This phenomenon is clearly evident in Figures 7b and S15, where a significantly increased loss factor and loss modulus and a wider damping temperature range were observed for LCE + BPAF and E-51 + BPAF resins. At the same time, the four epoxy resins barely lost weight before 300 °C as observed from the TGA curves, indicating good heat resistance. The maximum weight loss of LCE + BPAF and E-51 + BPAF occurred at 380–450 °C, which were higher than the 350–400 °C of LCE + DDM and E-51 + DDM (Figure 7c). This was ascribed to the high energy of C–F bonds in BPAF, which required a higher temperature to break. Additionally, LCE + BPAF, LCE + DDM, and E-51 + DDM resins showed relatively constant heat resistance indexes (T_{HRI})⁵⁷ of 176.9, 174.2, and 178.0 °C, while the E-51 + BPAF resin showed a slightly lower T_{HRI} of 169.1 °C. Besides, the LCE + DDM resin displayed the highest final carbon residue of 22.5%, while the E-51 + BPAF resin exhibited the lowest of 7.1%, which was consistent with the above analysis.

Hydrophobicity is also an essential property for electronic packaging and insulating materials, as water molecules in the surrounding environment will penetrate the material, which would increase the dielectric constant and dielectric loss, decrease the insulation and reliability, and speed up the deterioration of the materials. As displayed in Figure 7d, the water contact angle of the LCE + BPAF resin increased drastically to 91.5 from 73.3° of the E-51 + DDM resin, followed by 84.2 and 83.1° of E-51 + BPAF and LCE + DDM resins, respectively. The increased water contact angle was primarily caused by the fluorine-containing $-\text{CF}_3$ groups. This is because, in addition to the low polarizability, the fluorine atom is hydrophobic with a very low surface energy ascribed to the low interaction force with air. Furthermore, the ordered arrangement formed by the rigid biphenyl mesogens in LCE could inhibit water absorption, which also contributed to the improved hydrophobicity of the LCE + BPAF resin.

4. CONCLUSIONS

To conclude, a facile and scalable strategy to make epoxy resins simultaneously with high inherent thermal conductivity and

low dielectric performance by coupling the dual effect of liquid crystallinity and fluorine has been developed. The effect of the molecular structures of epoxy monomers and curing agents on intrinsic thermal conduction and dielectricity has been investigated. Owing to the dual effect of microscopically stacking of mesogens in LCE and the contribution of fluorine, ordered microstructures of the nematic liquid crystal phase were formed within the cross-linking network of the epoxy resins. Consequently, the phonon scattering was suppressed, and thus, the intrinsic thermal conductivity was improved. In addition, the very low polarizable $-\text{CF}_3$ groups in BPAF and the regular arrangement of LCE enabled the epoxy resin to achieve very low and stable ϵ and $\tan \delta$ at both low and high frequencies. The intrinsic thermal conductivity of LCE cured with the BPAF (LCE + BPAF) resin increased considerably to 0.38 W/(m·K), nearly twice as high as the 0.20 W/(m·K) of the commercial E-51 cured with DDM. Furthermore, the corresponding ϵ of the LCE + BPAF resin decreased remarkably from 3.40 to 2.72 while the $\tan \delta$ decreased from 0.044 to 0.038 at 10 GHz. Besides, the LCE + BPAF resin showed desirable electrical insulation, high thermal stability, and a much improved hydrophobicity. This work presents a convenient approach for breaking the bottleneck of making epoxy resins with both high intrinsic thermal conductivity and low dielectric performance that have been rarely investigated. Although there are some reported epoxy resins with singly higher intrinsic thermal conductivity or lower ϵ and $\tan \delta$, more complicated synthetic and purification procedures were employed (Table S1). This, however, lowers the benefit of thermal conductivity and low dielectricity. The prepared materials in this work are expected to be applied in various areas of electronic packaging, copper-clad plates, printed circuit boards, and semiconductors.

■ ASSOCIATED CONTENT

SI Supporting Information

The Supporting Information is available free of charge at <https://pubs.acs.org/doi/10.1021/jacsau.3c00582>.

Experimental methods; data analysis; ^1H NMR and ^{13}C NMR spectra of LCE; FT-IR spectra; dynamic DSC curves; digital images of different epoxy resins; XRD curves; POM images; thermal conductivities; ϵ and $\tan \delta$ values; loss modulus values; and comparison of intrinsic thermal conductivities, dielectric constant, and dielectric loss tangent of reported epoxy resins (PDF)

■ AUTHOR INFORMATION

Corresponding Author

Junwei Gu – Shaanxi Key Laboratory of Macromolecular Science and Technology, School of Chemistry and Chemical Engineering, Northwestern Polytechnical University, Xi'an, Shaanxi 710072, P. R. China; Chongqing Innovation Center, Northwestern Polytechnical University, Chongqing 401135, P. R. China; orcid.org/0000-0002-5792-0532; Email: gjw@nwpu.edu.cn, nwpugjw@163.com

Authors

Junliang Zhang – Shaanxi Key Laboratory of Macromolecular Science and Technology, School of Chemistry and Chemical Engineering, Northwestern Polytechnical University, Xi'an, Shaanxi 710072, P. R. China; Chongqing Innovation Center,

Northwestern Polytechnical University, Chongqing 401135, P. R. China; orcid.org/0000-0002-2630-4534

Lin Dang – Shaanxi Key Laboratory of Macromolecular Science and Technology, School of Chemistry and Chemical Engineering, Northwestern Polytechnical University, Xi'an, Shaanxi 710072, P. R. China; Chongqing Innovation Center, Northwestern Polytechnical University, Chongqing 401135, P. R. China

Fengyuan Zhang – Shaanxi Key Laboratory of Macromolecular Science and Technology, School of Chemistry and Chemical Engineering, Northwestern Polytechnical University, Xi'an, Shaanxi 710072, P. R. China; Chongqing Innovation Center, Northwestern Polytechnical University, Chongqing 401135, P. R. China

Kuan Zhang – Shaanxi Key Laboratory of Macromolecular Science and Technology, School of Chemistry and Chemical Engineering, Northwestern Polytechnical University, Xi'an, Shaanxi 710072, P. R. China; Chongqing Innovation Center, Northwestern Polytechnical University, Chongqing 401135, P. R. China

Qingqing Kong – Shaanxi Key Laboratory of Macromolecular Science and Technology, School of Chemistry and Chemical Engineering, Northwestern Polytechnical University, Xi'an, Shaanxi 710072, P. R. China; Chongqing Innovation Center, Northwestern Polytechnical University, Chongqing 401135, P. R. China

Complete contact information is available at:

<https://pubs.acs.org/10.1021/jacsau.3c00582>

Author Contributions

[§]J.Z. and L.D. contributed equally to this work. CRediT: **Junliang Zhang** conceptualization, data curation, formal analysis, funding acquisition, investigation, supervision, writing-original draft, writing-review & editing; **Lin Dang** data curation, formal analysis, investigation, writing-original draft; **Fengyuan Zhang** data curation, investigation; **Kuan Zhang** formal analysis, investigation, methodology; **Qingqing Kong** formal analysis, investigation; **Junwei Gu** formal analysis, funding acquisition, investigation, project administration, supervision, validation, writing-review & editing.

Notes

The authors declare no competing financial interest.

■ ACKNOWLEDGMENTS

This work was financially supported by the National Natural Science Foundation of China (21901208), the Natural Science Foundation of Chongqing, China (2023NSCQ-MSX2547), the China Postdoctoral Science Foundation (2022T150530), and the Fundamental Research Funds for the Central Universities. This work was also financially supported by the Polymer Electromagnetic Functional Materials Innovation Team of Shaanxi Sanqin Scholars. The authors would like to thank the Analytical & Testing Center of Northwestern Polytechnical University for the TGA test.

■ REFERENCES

- (1) Yang, Y.; Xu, Y.; Ji, Y.; Wei, Y. Functional epoxy vitrimers and composites. *Prog. Mater. Sci.* **2021**, *120*, No. 100710.
- (2) Duan, J.; Mei, C.; Wu, W.; Rao, L.; Fan, H.; Tang, Y.; Zhang, A. Disilyl Bis (Secondary Amine)-Enabled Epoxy Ring-Opening and Silylotropic N \rightarrow O Migration Leading to Low Dielectric Epoxy Copolymers. *Macromolecules* **2021**, *54*, 6947–6955.

- (3) Chen, X.; Wu, K.; Zhang, Y.; Liu, D.; Li, R.; Fu, Q. Tropocollagen-Inspired Hierarchical Spiral Structure of Organic Fibers in Epoxy Bulk for 3D High Thermal Conductivity. *Adv. Mater.* **2022**, *34*, No. 2206088.
- (4) Ruan, K.; Shi, X.; Zhang, Y.; Guo, Y.; Zhong, X.; Gu, J. Electric-Field-Induced Alignment of Functionalized Carbon Nanotubes Inside Thermally Conductive Liquid Crystalline Polyimide Composite Films. *Angew. Chem., Int. Ed.* **2023**, *62*, No. e202309010.
- (5) Huang, D.; Zhang, L.; Sheng, X.; Chen, Y. Facile strategy for constructing highly thermally conductive PVDF-BN/PEG phase change composites based on a salt template toward efficient thermal management of electronics. *Appl. Therm. Eng.* **2023**, *232*, No. 121041.
- (6) Wang, Z.; Wu, Z.; Weng, L.; Ge, S.; Jiang, D.; Huang, M.; Mulvihill, D. M.; Chen, Q.; Guo, Z.; Jassar, A.; He, X.; Zhang, X.; Xu, B. B. A Roadmap Review of Thermally Conductive Polymer Composites: Critical Factors, Progress, and Prospects. *Adv. Funct. Mater.* **2023**, *33*, No. 2301549.
- (7) Ma, T.; Ruan, K.; Guo, Y.; Han, Y.; Gu, J. Controlled length and number of thermal conduction pathways for copper wire/poly (lactic acid) composites via 3D printing. *Sci. China Mater.* **2023**, *66*, 4012–4021.
- (8) Zhang, L.; Deng, H.; Fu, Q. Recent progress on thermal conductive and electrical insulating polymer composites. *Compos. Commun.* **2018**, *8*, 74–82.
- (9) Moore, A. L.; Shi, L. Emerging challenges and materials for thermal management of electronics. *Mater. Today* **2014**, *17*, 163–174.
- (10) Zhang, F.; Feng, Y.; Feng, W. Three-dimensional interconnected networks for thermally conductive polymer composites: Design, preparation, properties, and mechanisms. *Mater. Sci. Eng., R* **2020**, *142*, No. 100580.
- (11) Han, Y.; Ruan, K.; Gu, J. Multifunctional Thermally Conductive Composite Films Based on Fungal Tree-like Heterostructured Silver Nanowires@Boron Nitride Nanosheets and Aramid Nanofibers. *Angew. Chem., Int. Ed.* **2023**, *62*, No. e202216093.
- (12) Zhang, Y.; Lei, C.; Wu, K.; Fu, Q. Fully Organic Bulk Polymer with Metallic Thermal Conductivity and Tunable Thermal Pathways. *Adv. Sci.* **2021**, *8*, No. 2004821.
- (13) Evans, A. M.; Giri, A.; Sangwan, V. K.; Xun, S.; Bartnof, M.; Torres Castanedo, C. G.; Balch, H. B.; Rahn, M. S.; Bradshaw, N. P.; Vitaku, E.; Burke, D. W.; Li, H.; Bedzyk, M. J.; Wang, F.; Brédas, J. L.; Malen, J. A.; McGaughey, A. J. H.; Hersam, M. C.; Dichtel, W. R.; Hopkins, P. E. Thermally conductive ultra-low-k dielectric layers based on two-dimensional covalent organic frameworks. *Nat. Mater.* **2021**, *20*, 1142–1148.
- (14) Zhang, Z.; Zhou, Y.; Yang, Y.; Ma, X.; Xuan, L.; Wu, X. Synthesis of tetra (epoxy)-terminated open-cage POSS and its particle thermo-crosslinking with diphenols for fabricating high performance low-k composites adopted in electronic packaging. *Compos. Sci. Technol.* **2023**, *231*, No. 109825.
- (15) Takeichi, T.; Furukawa, N. Epoxy Resins and Phenol-Formaldehyde Resins. In *Polymer Science: A Comprehensive Reference*; Elsevier, 2012; Vol. 5, pp 723–751.
- (16) Zhong, X.; Ruan, K.; Gu, J. Enhanced Thermal Conductivities of Liquid Crystal Polyesters from Controlled Structure of Molecular Chains by Introducing Different Dicarboxylic Acid Monomers. *Research* **2022**, *2022*, No. 9805686.
- (17) Kisiel, M.; Mossety-Leszczak, B. Development in liquid crystalline epoxy resins and composites-A review. *Eur. Polym. J.* **2020**, *124*, No. 109507.
- (18) Li, R.; Yang, X.; Li, J.; Shen, Y.; Zhang, L.; Lu, R.; Wang, C.; Zheng, X.; Chen, H.; Zhang, T. Review on polymer composites with high thermal conductivity and low dielectric properties for electronic packaging. *Mater. Today Phys.* **2022**, *22*, No. 100594.
- (19) Dong, X.; Wan, B.; Zheng, M. S.; Huang, L.; Feng, Y.; Yao, R.; Gao, J.; Zhao, Q. L.; Zha, J. W. Dual-effect Coupling for Superior Dielectric and Thermal Conductivity of Polyimide Composite Films Featuring “Crystal-like Phase” Structure. *Adv. Mater.* **2023**, No. 2307804.
- (20) Fu, F.; Zhou, X.; Shen, M.; Wang, D.; Xu, X.; Shang, S.; Song, Z. Q.; Song, J. Preparation of Hydrophobic Low-k Epoxy Resins with High Adhesion Using a Benzocyclobutene-Rosin Modifier. *ACS Sustainable Chem. Eng.* **2023**, *11*, 5973–5985.
- (21) Qian, X.; Zhou, J.; Chen, G. Phonon-engineered extreme thermal conductivity materials. *Nat. Mater.* **2021**, *20*, 1188–1202.
- (22) Jeong, I.; Kim, C. B.; Kang, D. G.; Jeong, K. U.; Jang, S. G.; You, N. H.; Ahn, S.; Lee, D. S.; Goh, M. Liquid crystalline epoxy resin with improved thermal conductivity by intermolecular dipole-dipole interactions. *J. Polym. Sci., Part A: Polym. Chem.* **2019**, *57*, 708–715.
- (23) Ruan, K.; Zhong, X.; Shi, X.; Dang, J.; Gu, J. Liquid crystal epoxy resins with high intrinsic thermal conductivities and their composites: A mini-review. *Mater. Today Phys.* **2021**, *20*, No. 100456.
- (24) Guo, H.; Zheng, J.; Gan, J.; Liang, L.; Wu, K.; Lu, M. High thermal conductivity epoxies containing substituted biphenyl mesogenic. *J. Mater. Sci.* **2016**, *27*, 2754–2759.
- (25) Zhong, X.; Yang, X.; Ruan, K.; Zhang, J.; Zhang, H.; Gu, J. Discotic Liquid Crystal Epoxy Resins Integrating Intrinsic High Thermal Conductivity and Intrinsic Flame Retardancy. *Macromol. Rapid Commun.* **2022**, *43*, No. 2100580.
- (26) Guo, H.; Lu, M.; Liang, L.; Wu, K.; Ma, D.; Xue, W. Liquid Crystalline Epoxies with Lateral Substituents Showing a Low Dielectric Constant and High Thermal Conductivity. *J. Electron. Mater.* **2017**, *46*, 982–991.
- (27) Kim, Y.; Yeo, H.; You, N. H.; Jang, S. G.; Ahn, S.; Jeong, K. U.; Lee, S. H.; Goh, M. Highly thermal conductive resins formed from wide-temperature-range eutectic mixtures of liquid crystalline epoxies bearing diglycidyl moieties at the side positions. *Polym. Chem.* **2017**, *8*, 2806–2814.
- (28) Dang, J.; Zhang, J.; Li, M.; Dang, L.; Gu, J. Enhancing intrinsic thermal conductivities of epoxy resins by introducing biphenyl mesogen-containing liquid crystalline co-curing agents. *Polym. Chem.* **2022**, *13*, 6046–6053.
- (29) Hong, Y. G.; Goh, M. Advances in Liquid Crystalline Epoxy Resins for High Thermal Conductivity. *Polymers* **2021**, *13*, No. 1302.
- (30) Islam, A. M.; Lim, H.; You, N. H.; Ahn, S.; Goh, M.; Hahn, J. R.; Yeo, H.; Jang, S. G. Enhanced Thermal Conductivity of Liquid Crystalline Epoxy Resin using Controlled Linear Polymerization. *ACS Macro Lett.* **2018**, *7*, 1180–1185.
- (31) Yuan, S. J.; Peng, Z. Q.; Rong, M. Z.; Zhang, M. Q. Enhancement of intrinsic thermal conductivity of liquid crystalline epoxy through the strategy of interlocked polymer networks. *Mater. Chem. Front.* **2022**, *6*, 1137–1149.
- (32) Volksen, W.; Miller, R. D.; Dubois, G. Low Dielectric Constant Materials. *Chem. Rev.* **2010**, *110*, 56–110.
- (33) Yu, Z.; Du, X.; Zhu, P.; Zhao, T.; Sun, R.; Chen, J.; Wang, N.; Li, W. Surface modified hollow glass microspheres-epoxy composites with enhanced thermal insulation and reduced dielectric constant. *Mater. Today Commun.* **2022**, *32*, No. 104046.
- (34) Zhang, J.; Wang, C.; Feng, W.; Tang, Y. Cyanate ester resins with superior dielectric, mechanical, and flame retardance properties obtained by introducing a fluorinated hyperbranched polyaryletherketone. *Polym. Chem.* **2022**, *13*, 2484–2494.
- (35) Wang, C.; Tang, Y.; Zhou, Y.; Zhang, Y.; Kong, J.; Gu, J.; Zhang, J. Cyanate ester resins toughened with epoxy-terminated and fluorine-containing polyaryletherketone. *Polym. Chem.* **2021**, *12*, 3753–3761.
- (36) Zhou, D. L.; Li, J. H.; Guo, Q. Y.; Lin, X.; Zhang, Q.; Chen, F.; Han, D.; Fu, Q. Polyhedral Oligomeric Silsesquioxanes Based Ultralow-k Materials: The Effect of Cage Size. *Adv. Funct. Mater.* **2021**, *31*, No. 2102074.
- (37) Wu, M. G.; Liu, X.; Zhou, Y.; Fu, L.; Pan, J.; Cao, B.; Liu, S.; Zhao, J.; Xie, W. Fluorinated anhydride-terminated imide oligomers toward high-performance epoxy thermosets enabled by hydroxyl elimination and low dielectric polarizability strategy. *Chem. Eng. J.* **2022**, *437*, No. 135435.
- (38) Liu, X.; Xiao, Z.; Liu, X.; Liu, Y.; Zhao, J.; Liu, S. Design and synthesis of epoxy prepolymer containing aromatic imide structures

for thermoset with excellent thermal, mechanical and dielectric properties. *Chem. Eng. Sci.* **2023**, *281*, No. 119149.

(39) Li, C.; Fan, H.; Aziz, T.; Bittencourt, C.; Wu, L.; Wang, D. Y.; Dubois, P. Biobased Epoxy Resin with Low Electrical Permissivity and Flame Retardancy: From Environmental Friendly High-Throughput Synthesis to Properties. *ACS Sustainable Chem. Eng.* **2018**, *6*, 8856–8867.

(40) Hou, J.; Sun, J.; Fang, Q. Oxygen-free polymers: new materials with low dielectric constant and ultra-low dielectric loss at high frequency. *Polym. Chem.* **2023**, *14*, 3203–3212.

(41) Na, T.; Jiang, H.; Liu, X.; Zhao, C. Preparation and properties of novel fluorinated epoxy resins cured with 4-trifluoromethyl phenylbenzimidazole for application in electronic materials. *Eur. Polym. J.* **2018**, *100*, 96–102.

(42) Xing, A.; Bao, F.; Fu, J.; Miao, X.; Liu, T.; Zhai, H.; Cao, X.; Meng, Y.; Li, X. Tertiary-amine-free, non-planar, fluorine-containing tetrafunctional epoxy and its application as high performance matrix. *Polym. Test.* **2018**, *71*, 38–48.

(43) Luo, H.; Zhang, D.; Jiang, C.; Yuan, X.; Chen, C.; Zhou, K. Improved Dielectric Properties and Energy Storage Density of Poly (vinylidene fluoride-co-hexafluoropropylene) Nanocomposite with Hydantoin Epoxy Resin Coated BaTiO₃. *ACS Appl. Mater. Interfaces* **2015**, *7*, 8061–8069.

(44) Gong, H.; Wu, J.; Zhao, Z.; Guo, Z.; Gao, L.; Zhang, B.; Li, M. H.; Hu, J. Recyclable high-performance glass-fiber/epoxy composites with UV-shielding and intrinsic damage self-reporting properties. *Chem. Eng. J.* **2022**, *446*, No. 137392.

(45) Chen, M.; Zhou, L.; Wu, Y.; Zhao, X.; Zhang, Y. Rapid Stress Relaxation and Moderate Temperature of Malleability Enabled by the Synergy of Disulfide Metathesis and Carboxylate Transesterification in Epoxy Vitrimers. *ACS Macro Lett.* **2019**, *8*, 255–260.

(46) Xu, S.; Zhou, J.; Pan, P. Strain-induced multiscale structural evolutions of crystallized polymers: From fundamental studies to recent progresses. *Prog. Polym. Sci.* **2023**, *140*, No. 101676.

(47) Giang, T.; Kim, J. Effect of Liquid-Crystalline Epoxy Backbone Structure on Thermal Conductivity of Epoxy-Alumina Composites. *J. Electron. Mater.* **2017**, *46*, 627–636.

(48) Zhang, Y.; Liu, Z.; Zhang, X.; Guo, S. Sandwich-Layered Dielectric Film with Intrinsically Excellent Adhesion, Low Dielectric Constant, and Ultralow Dielectric Loss for a High-Frequency Flexible Printed Circuit. *Ind. Eng. Chem. Res.* **2021**, *60*, 11749–11759.

(49) Yang, D.; Ni, Y.; Kong, X.; Gao, D.; Wang, Y.; Hu, T.; Zhang, L. Mussel-inspired modification of boron nitride for natural rubber composites with high thermal conductivity and low dielectric constant. *Compos. Sci. Technol.* **2019**, *177*, 18–25.

(50) Maier, G. Low dielectric constant polymers for micro-electronics. *Prog. Polym. Sci.* **2001**, *26*, 3–65.

(51) Luo, Y.; Jin, K.; He, C.; Wang, J.; Sun, J.; He, F.; Zhou, J.; Wang, Y.; Fang, Q. An Intrinsically Microporous Network Polymer with Good Dielectric Properties at High Frequency. *Macromolecules* **2016**, *49*, 7314–7321.

(52) Yin, X.; Feng, Y.; Zhao, Q.; Li, Y.; Li, S.; Dong, H.; Hu, W.; Feng, W. Highly transparent, strong, and flexible fluorographene/fluorinated polyimide nanocomposite films with low dielectric constant. *J. Mater. Chem. C* **2018**, *6*, 6378–6384.

(53) Liu, Z.; Fan, X.; Cheng, L.; Zhang, J.; Tang, L.; Tang, Y.; Kong, J.; Gu, J. Hybrid Polymer Membrane Functionalized PBO Fibers/Cyanate Esters Wave-Transparent Laminated Composites. *Adv. Fiber Mater.* **2022**, *4*, 520–531.

(54) Tang, L.; Tang, Y.; Zhang, J.; Lin, Y.; Kong, J.; Zhou, K.; Gu, J. High-strength super-hydrophobic double-layered PBO nanofiber-polytetrafluoroethylene nanocomposite paper for high-performance wave-transparent applications. *Sci. Bull.* **2022**, *67*, 2196–2207.

(55) Ye, N.; Li, J.; Zhang, G.; Lu, Y.; Wang, Z.; Zhang, H.; Lu, Y. Vitriimer-Assisted Construction of Boron Nitride Vertically Aligned Nacre-mimetic Composites for Highly Thermally Conductive Thermal Interface Materials. *Chem. Mater.* **2023**, *35*, 5193–5203.

(56) Schweitzer, J.; Merad, S.; Schrodj, G.; Bally-Le Gall, F.; Vonna, L. Determination of the Crosslinking Density of a Silicone Elastomer. *J. Chem. Educ.* **2019**, *96*, 1472–1478.

(57) Wang, X.; Cao, W.; Su, Z.; Zhao, K.; Dai, B.; Gao, G.; Zhao, J.; Zhao, K.; Wang, Z.; Sun, T.; Han, J.; Zhu, J. Fabrication of High Thermal Conductivity Nanodiamond/Aramid Nanofiber Composite Films with Superior Multifunctional Properties. *ACS Appl. Mater. Interfaces* **2023**, *15*, 27130–27143.